Energy partition in C_{60}-diamond-(111)-surface collisions: A molecular-dynamics simulation

P. Blaudeck and Th. Frauenheim
Department of Physics, University of Chemnitz-Zwickau, D-09009 Chemnitz, Germany

H.-G. Busmann and T. Lill
Freiburger Materialforschungsinstitut der Universitaet, D-79104 Freiburg, Stefan-Meier-Strasse 31a, Germany
(Received 6 August 1993; revised manuscript received 26 October 1993)

Collisions of C_{60} with hydrogen-terminated diamond-(111) surfaces were studied by molecular-dynamics simulations based on a semiempirical density-functional approach. The dominating factor determining the energy partition in the C_{60}-diamond-(111)-surface collision at constant impact energy is the orientation of the molecules relative to the initial impact points on the surface. In agreement with the experimental results using velocity-selective time-of-flight mass spectroscopy the center-of-mass kinetic energies after the collisions are distributed around a mean value which is only slightly affected by the initial impact energy. The final energy content of the C_{60}'s increases with the incident kinetic energy, depends strongly on the impact scattering topology, and yields a narrow distribution with increasing mean values in correlation with lower center-of-mass kinetic energies.

I. INTRODUCTION

Studies that analyze the dissociation products of hot polyatomic molecules are of high scientific interest, since they are directly related to the unimolecular reaction dynamics of their desintegration. An entire interpretation of its results is only possible if one characterizes the excitation step of the molecule. A direct vibrational excitation is achieved in molecule-surface scattering. Experiments[1–4] have shown that the molecules dissociate; a process named surface-induced dissociation (SID). Since the distribution of the internal energy is much narrower for molecules heated by SID as compared to gas phase collisions,[5] it is to the benefit of SID that the abundant distributions of the dissociation products correspond to relatively well defined internal energies.

In recent years, scattering of fullerene ions at crystalline surfaces has proved to be a well-suited model system for surface collision induced excitation of polyatomic molecules.[6–10] Moreover, relevant carbon and hydrogen-carbon systems can now realistically be simulated by molecular-dynamics (MD) calculations, which are based on quantum mechanically derived forces.[11,12] Such calculations have been extended here to simulate scattering of fullerenes at a diamond (111) surface and are compared to the experimental results obtained for scattering at diamond (111) and graphite (0001).[13] Simulations, that are based on *empirical* potentials, have already given a quantitative description of the scattering process.[14] However, the data obtained for the final kinetic energy in their values deviate from the experimental data in Ref. 13.

To improve the understanding of the complex and highly reactive scattering processes, MD simulations on the basis of more realistic quantum mechanically derived potentials have been performed for a detailed comparison with the experiments. The experimental results will be summarized briefly in Sec. II. The *semiempirical* density-functional (DF) aproach for MD, the scattering geometry, and the applied simulation regime are described in Sec. III. In Sec. IV we present the results on the scattering dynamics, the energy partition during collision, and discuss reactive states of the C_{60}'s molecules with the diamond surface. Concluding in Sec. V, we compare our simulation results with the experiments and quantitative data derived by applying *empirical* potential MD.

II. EXPERIMENTAL RESULTS

The energy partition in collisions of C_{60}^+ ions with diamond (111) and graphite (0001) surfaces has recently been reported.[13] Figure 1 shows the final velocity distri-

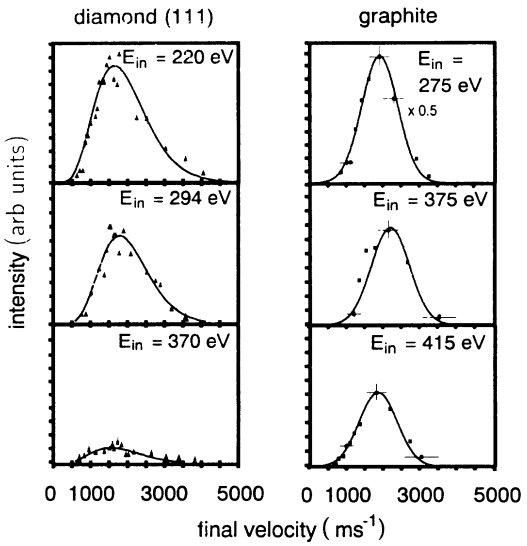

FIG. 1. Velocity distributions of scattered C_{60}^+ ions from diamond (111), left panel, and graphite (0001), right panel, for various impact energies, E_{in}, at the maximum of the corresponding angular distribution (Ref. 13). The individual data points are experimental results and the solid lines are analytical functions fitted to the data.

butions for different initial impact energies E_{in}. At a first glance, they do not depend on the impact energy and are very similar for the two targets. The distributions range from about 500 m/s to 4000 m/s corresponding to final center-of-mass kinetic energies E_{kin}^{cm} ranging from about 1 eV to 60 eV, respectively. The maximum is found at about 1750 m/s (11.4 eV). The fullerene molecules come strongly heated off the surface yielding their metastable fragmentation. The rate of fragmentation has been analyzed as a function of E_{in} and E_{kin}^{cm}. It was found that collisional heating increases with increasing E_{in} at constant E_{kin}^{cm}, and with increasing E_{kin}^{cm} at constant E_{in}; the increase in temperature varies with increasing speed. In a next step, the ratio of the final internal energy to the energy barrier height for dissociation, E_f^*/D, has been estimated by using a RRK formalism.[10] Figure 2(a) shows this ratio as a function of E_{kin}^{cm} at various values of E_{in}. It is visible that E_f^*/D increases with increasing E_{kin}^{cm}, however, it seems to approach a saturation value of about 8. Figure 2(b) shows the same ratio for E_{in} at $E_{kin}^{cm} = 11.4$ eV and 23.3 eV. A linear increase can be seen. It should be noted that the scattering signal is already very low at $E_{in} = 450$ eV,[13] which is possibly owing to an upper limit of this ratio for molecules that come off the surface without disintegration.

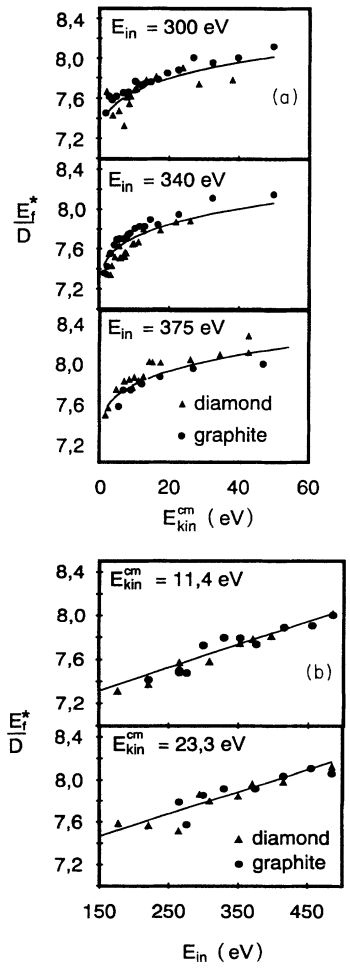

FIG. 2. Rate of metastable fragmentation of C_{60}^+ ions after scattering off a diamond (111) and graphite (0001) surface (a) as a function of the center-of-mass kinetic energy, E_{kin}^{cm}, for different E_{in} and (b) in dependence on the initial impact energy, E_{in}, for different E_{kin}^{cm}.

III. COMPUTATIONAL METHOD AND GEOMETRY

The computational method and scattering geometry used for the present calculations now will be briefly described. The dynamical simulations of these hyperthermal scattering processes between the C_{60} molecules and crystalline surfaces are based on quantum mechanically derived interatomic forces, considering the electronic structure of the cluster-surface system explicitly by the use of a semiempirical MD density-functional (DF) approach, originally introduced for cluster studies.[15]

The electronic wave functions [Kohn-Sham orbitals $\psi(\mathbf{r})$] are written as linear combinations of atomic orbitals $\varphi_\mu(\mathbf{r}-\mathbf{R}_l)$, centered at the nuclei (LCAO ansatz), which are determined *self-consistently* using the local density approximation (LDA): $\psi(\mathbf{r}) = \sum_\mu c_\mu \varphi_\mu(\mathbf{r}-\mathbf{R}_l)$. Within a minimal basis representation the localized s and p valence electron wave functions were considered in the LCAO ansatz. Each wave function is represented by a set of 12 Slater-type functions. By the use of a simplified DF scheme the effective one-particle potential V_{eff} in the Kohn-Sham *Hamiltonian* $\hat{h} = \hat{t} + V_{eff}(\mathbf{r})$ is approximated as a sum of potentials of neutral atoms. Consistent with this approximation one has to neglect several contributions to the *Hamiltonian* matrix elements $h_{\mu\nu}$ in the *secular* equation for solving the electron problem for cluster electron eigenenergies and wave functions: $\sum_\mu c_\mu^i (h_{\mu\nu} - \varepsilon_i S_{\mu\nu}) = 0$, see Refs. 12 and 15. The total energy of the system as a function of the atomic coordinates now can be decomposed into two contributions, $E_{tot}(\{\mathbf{R}_l\}) = E_{bind}(\{\mathbf{R}_l\}) + E_{rep}(\{\mathbf{R}_l - \mathbf{R}_k\})$. The first term as the sum over all occupied cluster electron energies represents the *so-called* band structure energy and the second, as a repulsive energy, includes the core-core repulsions between the atoms and interactions between electrons at different lattice sites that partly compensate. As a further approximation this repulsive energy is modeled by short range repulsive *empirical* two-particle potentials (polynomials of fifth order), which are fitted to reproduce the potential energy curves of the corresponding two-atomic molecules in dependence on a wide range of the interatomic separation, $\geq 1.3a_B$ (Bohr radius), and thus allows for MD simulations of atomic configurations that are far from equilibrium. This procedure improves the fitting scheme reported in Refs. 11 and 12, where the first attempts were made in simply reproducing the two-atomic equilibrium separations and the experimental vibrational frequencies. The interatomic forces on each atom are derived from the gradients of the total energy at the considered atom sites. This scheme may be viewed as a *hybrid* between *ab initio* molecular dynamics, based on density functional theory (DFT) and the use of purely *empirical* potentials. It has the ad-

vantage over the latter of overcoming the transferability problem, where parametrized potentials based on experimental data or molecular *ab initio* calculations can be difficult to transfer from one system to another. On the other hand, it requires less computational effort than *ab initio* molecular dynamics. A more detailed description of the method is given elsewhere, e.g., Refs. 12 and 15. The reliability of the method has been tested and characterized to the problems of interest. In particular, it has been proven that representative carbon and hydrocarbon structures (microclusters, molecules, fullerenes, bulk crystalline, amorphous modifications, and surfaces) are quantitatively reproduced in geometry, in structure data, and in the relative differences of the cohesive energies of different structures.[11,12] Newton's equation of atomic motion in the MD is integrated numerically during the simulations by the use of the Verlet algorithm. A time step of 10 atu (1 atu = 2.4×10^{-17} sec) has been proven to guarantee the conservation of energy over the entire time of the simulation.

All computational experiments have been performed by using a two-dimensional periodic thin surface slab supercell of (111) diamond with hydrogen bonded at both sides. The carbon atoms of the bottom surface are fixed at their positions to simulate an infinite crystal. The dynamics of the system (upper substrate layers—molecule) then are simulated to study the energy partition and chemical reactions during the scattering process. To minimize the computational effort we have checked how many double layers of the diamond crystal have to be taken into account. In all cases, scattering and motion of the C_{60} has been described sufficiently well by only two double layers of diamond. The diamond surface is much more rigid than the C_{60} and it has been found that by using a diamond target with an additional double-layer the simulation yields nearly no change in the response of the surface to the C_{60}. Therefore, an additional third double layer did not cause any significant improvement, as it will also be shown below—compare Figure 5.

IV. SIMULATION RESULTS

The atoms of the C_{60} molecule were initially located at the vertices of a truncated icosahedron corresponding to $T = 0$ K at a sufficient distance above the surface to have no interaction with the surface atoms. A translational velocity component was added to each atom to give E_{in} = 150, 200, and 300 eV at an impact angle of 20° with respect to the surface normal. Different initial orientations as well as positions of the C_{60} with respect to the surface have been considered, i.e., orientations such that the molecules first touch the surface with a hexagon, pentagon, and C-C bond. It turned out that the microscopic topology during scattering (influenced by the orientation of the C_{60} and its starting position) is one of the most important parameters of the scattering process. In Fig. 3 two cases, with the same initial position of the center of mass, (a) pentagon down, (b) hexagon down, are compared at the time of greatest deformation. In case (a) most of the topological structure is kept but in case (b) a lot of new bonds appear resulting in a highly disordered cluster. On the other hand, the variation of the point of impact on the surface has also shown the same significant effect. The total kinetic energy E_{kin}^{tot} and the center-of-mass kinetic energy E_{kin}^{cm} as a function of time, following the trajectories, are shown in Fig. 4 for different values of E_{in} and two initial orientations. The total kinetic energy E_{kin}^{tot} (solid and dotted lines) represents the sum of

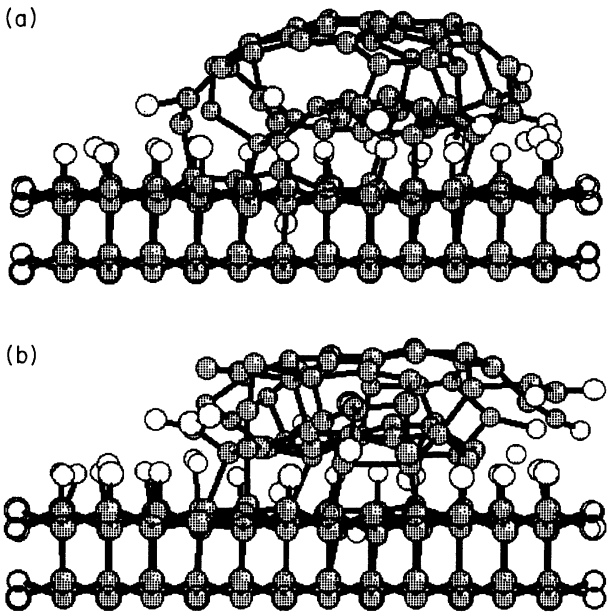

FIG. 3. C_{60} in the most deformed configuration during the collision; (a) pentagon down and (b) hexagon down, E_{in} = 300 eV.

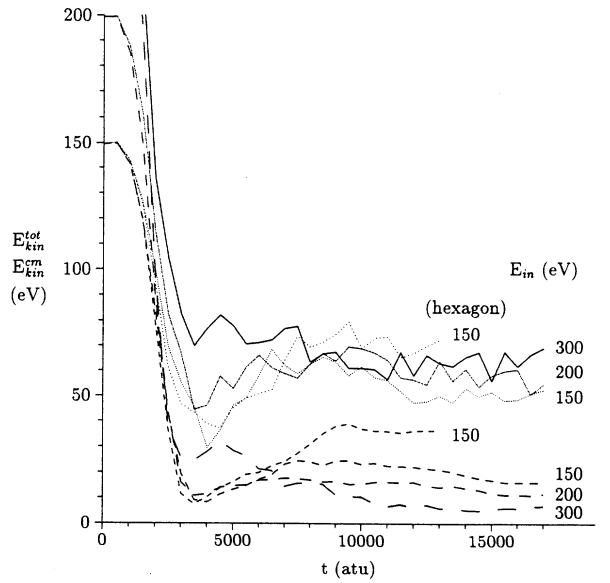

FIG. 4. Characteristic kinetic energies as a function of time. Total kinetic energy of the C_{60} molecule/cluster, E_{kin}^{tot} (solid and dotted lines) and C_{60} center-of-mass kinetic energy, E_{kin}^{cm} (dashed lines): Three trajectories for a pentagon orientation parallel to the surface at different primary impact kinetic energies E_{in} and one trajectory for a hexagon orientation.

the kinetic energies of all C_{60} atoms, and its differences to E_{kin}^{cm} (dashed lines) is considered in the following as half of its internal energy. So, including also the potential energy due to the deformation of the C_{60} molecules via using the virial theorem the internal energy becomes $E_f^* = 2(E_{kin}^{tot} - E_{kin}^{cm})$.

The partition of E_{in} is particularly dependent on the initial state. The trajectories for $E_{in} = 150$ eV, visible in Fig. 4, show that E_{kin}^{cm} is much higher when, for this example, the molecule first touches the surface with a hexagon than with a pentagon. The absolute values are about 75 eV and 55 eV for E_{kin}^{tot}, 34 and 20 eV for E_{kin}^{cm}, and hence 82 and 70 eV for E_f^*. The energy tranferred to the target may be estimated as $E_{tar} = E_{in} - E_f^* - E_{kin}^{cm}$. Thus, the collisions are extremely inelastic as it is found in the experiments. The data also corraborate the assumption[13] that the increase in C_{60} temperature with increasing speed at constant E_{in} is due to different initial states of the molecules.

Now when E_{in} is increased in the calculations, an increase of the energy left into the molecule is observed. In some cases, strongly reactive collisions have been obtained. Figure 5 monitors one example of an absorption process. Starting with an energy at 300 eV and a hexagon parallel to the surface, a lot of bonds are formed between the C_{60} and the diamond double layer, such that the C_{60} is deposited as an amorphous cluster. To confirm that this is not an effect of a too small elastic response of the target due to the limited target extension in depth, the same simulation has been performed with one additional double layer of diamond. The corresponding trajectories are also shown in Fig. 5. There is no relevant difference between the calculations made with two and three atomic double layers in this case and holds true in lower energy collisions when the molecule rebounds from the surface. The test also has shown that in both cases the elongation of the first surface layer followed in time is approximately the same.

The distribution of the final internal energies and the final center-of-mass energies dependent on the impact energy for all simulated collisions is shown statistically in Fig. 6. All results with the same impact angle (20°) seem to be within the hypothetical limits which are drawn by dotted lines into the figure. No scattering event outside this range has been detected. As a qualitative argument supporting this the changing behavior in the scattering from almost elastic to deeply inelastic with an increase of the initial C_{60} energy should be discussed. These limits depend strongly on the impact angle as it is shown by the two examples for $\alpha = 45°$. For energies up to 100 eV the dominating part of the impact energy is still contained in the reflected C_{60}. Note that for the case when the molecule remains at the surface ($E_{kin}^{cm} \approx 0$), the internal energy is measured before the thermodynamic equilibrium has been reached. Although all collisions for $150 < E_{in} < 300$ eV are reactive, in that sputtering of hydrogen from the surface occurs, scattering of $C_{60\pm5}$ is observed in the cases, shown in Fig. 4, where E_{kin}^{tot} and E_{kin}^{cm} of the corresponding trajectories are shown. The mean final values of these energies representing an average over all trajectories leading to $C_{60\pm5}$ at each initial energy are plotted in Fig. 7 where they are compared to corresponding values given by Mowrey *et al.*,[14] who also report on the formation of temporary bonds between the C_{60} and the surface during the collision. Although we have found a slight decrease in E_{kin}^{cm} of C_{60} as a function of E_{in} at a fixed scattering topology (cf. Fig. 4), it is worth noting that the values agree surprisingly well with the mean values of E_{kin}^{cm} for all product species (cf. Fig. 6) and with the range of the experimental maxima of E_{kin}^{cm} (dark rectangle) in Fig. 7. At the same time,

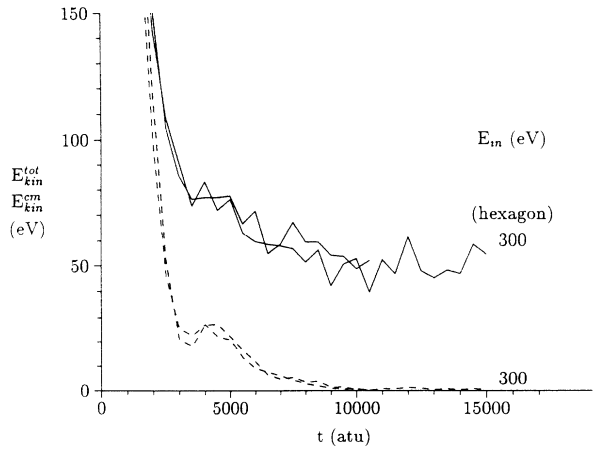

FIG. 5. Energy partition of a C_{60} molecule deposited at $E_{in} = 300$ eV as a function of time. Total kinetic energy of the C_{60} molecule/cluster, E_{kin}^{tot} (solid and dotted lines) and C_{60} center-of-mass kinetic energy, E_{kin}^{cm} (dashed lines). The two different curves correspond to situations where two and three diamond double carbon layers have been included in the dynamical simulation.

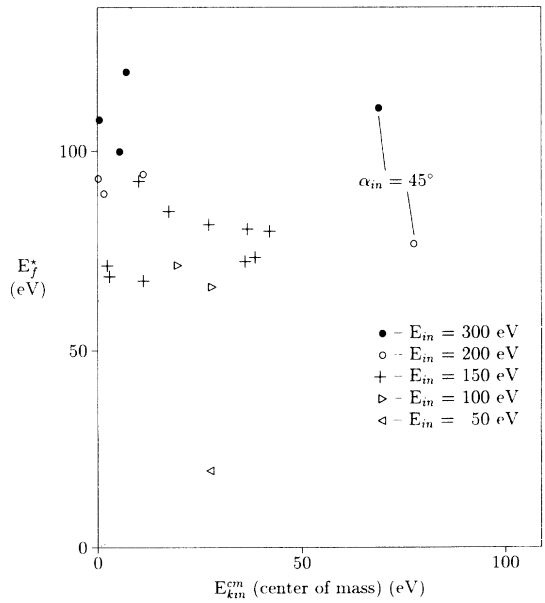

FIG. 6. Statistics of the final energies of all product species for different initial energies for an impact angle of 20° with respect to the surface normal. The dotted lines indicate the expected lower and upper limits. Two cases with a larger impact angle are included.

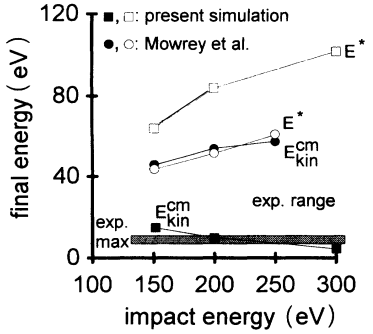

FIG. 7. Mean values of the final internal, E_f^*, and center-of-mass kinetic energies, $E_{\rm kin}^{\rm cm}$, as a function of the initial impact energy, $E_{\rm in}$, for all trajectories leading to scattered $C_{60\pm5}$. The present simulations are compared to those of Mowrey *et al.* (Ref. 14) and to the experiments. —□—, —○—: E_f^* and —■—, —●—: $E_{\rm kin}^{\rm cm}$ of the present and the simulation of Mowrey *et al.*, respectively. Bright rectangle: Range of the experimental $E_{\rm kin}^{\rm cm}$ distributions as a function of $E_{\rm in}$. Dark rectangle: Maxima of the experimental $E_{\rm kin}^{\rm cm}$ distributions as a function of $E_{\rm in}$.

E_f^* for C_{60} increases with increasing $E_{\rm in}$ (cf. Fig. 7), which is also consistent with the experimental values of E_f^*/D, shown in Fig. 2, whereas the mean center-of-mass kinetic energies $E_{\rm kin}^{\rm cm}$ for all species are almost independent of $E_{\rm in}$ (cf. Fig. 6). This is consistent with the experimental results of Fig. 1. The results of Mowrey *et al.*[14] for $E_{\rm kin}^{\rm cm}$ deviate considerably from our determined values. They are also much too high when compared to the experiment, and their internal energies are too low. This difference might be due to applying the *empirical* potential concept to structure configurations which are far from equilibrium, e.g., for situations for which they actually have not been derived. Thus, MD simulated annealing (SA) studies, where the interatomic forces have a quantum mechanical origin, starting from *first principle* ideas, give better quantitative results for the final energies. But in a related paper,[16] Mowrey *et al.* also reported that at the highest impact energies most collisions are highly reactive yielding low $E_{\rm kin}^{\rm cm}$ ($\approx$ 10 eV) and high internal energies ($\approx$ 80 eV), in the cases that are comparable to our results.

The interactions of the C_{60} molecules with the surface and the related scattering characteristics may be described as follows: (1) At $E_{\rm in} \approx 150$ eV, reactive chainlike carbon segments of a slightly destorted C_{60} cluster form single bonds with radical surface sites before leaving the surface. After the molecules have left the surface, a tendency to reorganize in time has been observed. Hydrogens which are bonded at the leaving C_{60} molecules are pushed away during the reorganization. The reason for this may be found in the nonuniform distribution of the kinetic energy in large clusters which causes C-H bond breaking as the result of local excitations that have been really observed during the simulations within the considered time scale. (2) At $E_{\rm in} \approx 200$ eV, small rings as well as chainlike structures are formed which are typical for small carbon clusters. After the molecules have left the surface as $C_{60\pm5}$, a reorganization into the original C_{60} structure is not observed on the investigated time scale. (3) At higher energies, $E_{\rm in} \approx 300$ eV, the C_{60} molecules completely lose their geometry and bonding configuration.

They come from the surface as $C_{60\pm5}$ amorphous clusters which are strongly heated and fragmentate in time or remain permanently bonded to the substrate layer. (4) For $E_{\rm in} > 300$ eV, all molecules are deposited onto the surface forming amorphous carbon structures.

V. CONCLUSION

The theoretical result of the energy partition during the collision has shown that $E_{\rm kin}^{\rm cm}$ of C_{60} molecules at fixed scattering topology (cf. Fig. 4), and their mean values, $\bar{E}_{\rm kin}^{\rm cm}$, averaged over the number of trajectories (cf. Fig. 7) slightly decreases with increasing $E_{\rm in}$ for lower values, remaining nearly constant for higher values. Simultaneously, in agreement with the experiment we observe an increase of E_f^* with increasing $E_{\rm kin}^{\rm cm}$ at constant $E_{\rm in}$ as well as with increasing $E_{\rm in}$ at constant $E_{\rm kin}^{\rm cm}$. For some initial configurations it was found that C_{60} scattering occurs only for $E_{\rm in} \leq 150$ eV. Higher values for $E_{\rm in}$ give rise to a dissociation of the molecules during the collision. This describes the experimental data pretty well, compare Figs. 1 and 2, and directly yields an interpretation of the general experimental results. The impacting ions neutralize during the collisions, and the scattered positively charged molecules are those which undergo delayed, thermionic electron emission,[17] i.e., those which have fullerene structure after the collision. Furthermore, it has been shown that $E_{\rm kin}^{\rm cm}$ and E_f^* are correlated. The ratio E_f^*/D as deduced from the experiments seem to approach a saturation value. This has been confirmed by the simulation results presented in Fig. 6 giving strong evidence that scattering of C_{60} fullerenes is only realized up to an upper bound of E_f^* in correlation with an upper bound for $E_{\rm kin}^{\rm cm}$ for the scattered C_{60} fullerenes. This upper bound strongly depends on the impact angle, and therefore, on the experimental conditions.

One consequence of the present simulation is that the scattered positive ions observed in the experiments are probably those which accidentally are scattered with suitable initial states. Most of the molecules disintegrate in the collision, where the fragments are either adsorbed at the surface or come from the surface as neutrals or negative ions. The simulations have essentially improved our understanding of the experimental results. In particular, it has been shown that the intial position and orientation of the molecule is the dominating parameter for the energy partition in the collision process. This effect is expected to occur also in cases when other molecules such as peptides or small molecules are scattered at a surface.

ACKNOWLEDGMENTS

Sincere thanks are due to I. V. Hertel with whom we had many stimulating discussions. Some of the computations were performed using the Cray at the HLRZ, KFA Jülich GmbH.

[1] W. Eckstein, H. Verbeck, and S. Datz, Appl. Phys. Lett. **27**, 527 (1975).
[2] W. Heiland and E. Taglauer, Nucl. Instrum. Methods **194**, 667 (1982).
[3] R. G. Cooks, T. Ast, and J. H. Beynon, Int. J. Mass Spectrom. Ion Proc. **16**, 348 (1975).
[4] R. M. Gandy, R. Ampulaski, J. Prusaczyk, and R. H. Johnson, Int. J. Mass Spectrom. Ion Phys. **24**, 363 (1977).
[5] R. G. Cooks, T. Ast, and M. D. A. Mabud, Int. J. Mass Spectrom. Ion Phys. **100**, 209 (1990).
[6] S. W. McElvany, M. M. Ross, and J. H. Callahan, in *Clusters and Cluster-Assembled Materials*, edited by R. S. Averback, J. Bernholc, and D. L. Nelson, MRS Symposia Proceedings No. 206 (Materials Research Society, Pittsburgh, 1991), p. 697.
[7] R. D. Beck, P. M. St. John, M. M. Alvarez, F. Diederich, and R. L. Whetten, J. Phys. Chem. **95**, 220 (1991).
[8] H.-G. Busmann, Th. Lill, and I. V. Hertel, Chem. Phys. Lett. **187**, 459 (1991).
[9] Th. Lill, H.-G. Busmann, B. Reif, and I. V. Hertel, Appl. Phys. A **55**, 461 (1992).
[10] H.-G. Busmann, Th. Lill, B. Reif, and I. V. Hertel, Surf. Sci. **272**, 146 (1992).
[11] Th. Frauenheim and P. Blaudeck, Appl. Surf. Sci. **60/61**, 281 (1992).
[12] P. Blaudeck, Th. Frauenheim, D. Porezag, G. Seifert, and E. Fromm, J. Phys. Condens. Matter **4**, 6389 (1992).
[13] H.-G. Busmann, Th. Lill, B. Reif, I. V. Hertel, and H. G. Maguire, J. Chem. Phys. **98**, 7574 (1993).
[14] R. C. Mowrey, D. W. Brenner, B. I. Dunlap, J. W. Mintmire, and C. T. White, J. Phys. Chem. **95**, 7138 (1991).
[15] G. Seifert and H. Eschrig, Phys. Status Solidi B **127**, 573 (1985); G. Seifert, H. Eschrig, and W. Ziegert, Z. Phys. Chem. (Leipzig) **267**, 529 (1986); G. Seifert and R. O. Jones, Z. Phys. D **20**, 77 (1991).
[16] R. C. Mowrey, D. W. Brenner, B. I. Dunlap, J. W. Mintmire and C. T. White, in *Clusters and Cluster-Assembled Materials* (Ref. 6), p. 357.
[17] Ch. Yeretzian and R. L. Whetten, Z. Phys. D (to be published).

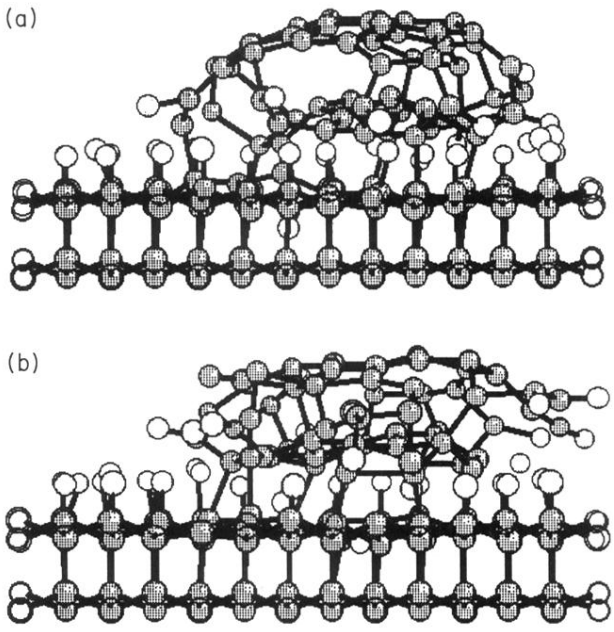

FIG. 3. C_{60} in the most deformed configuration during the collision; (a) pentagon down and (b) hexagon down, $E_{in} = 300$ eV.